



**HAL**  
open science

## **Instrumented indentation for determining stress and strain levels of prestrained DC01 sheets**

Mohamad Idriss, Olivier Bartier, Dominique Guines, Lionel Leotoing, Gérard Mauvoisin, Xavier Hernot

► **To cite this version:**

Mohamad Idriss, Olivier Bartier, Dominique Guines, Lionel Leotoing, Gérard Mauvoisin, et al.. Instrumented indentation for determining stress and strain levels of prestrained DC01 sheets. *International Journal of Mechanical Sciences*, 2023, 238, pp.107833. 10.1016/j.ijmecsci.2022.107833 . hal-03903807

**HAL Id: hal-03903807**

**<https://univ-rennes.hal.science/hal-03903807v1>**

Submitted on 16 Dec 2022

**HAL** is a multi-disciplinary open access archive for the deposit and dissemination of scientific research documents, whether they are published or not. The documents may come from teaching and research institutions in France or abroad, or from public or private research centers.

L'archive ouverte pluridisciplinaire **HAL**, est destinée au dépôt et à la diffusion de documents scientifiques de niveau recherche, publiés ou non, émanant des établissements d'enseignement et de recherche français ou étrangers, des laboratoires publics ou privés.

# Highlights

- Voce law is determined at different strain levels using instrumented indentation
- The proposed approach predicts correctly the stress state of pre-strained specimens
- Pre-strain states are also predicted correctly for strain values not exceeding 15 %
- This is validated for monotonic and cyclic pre-loading paths i.e. shear and Marciniak
- In cyclic loading, results are improved when considering kinematic hardening

Journal Pre-proof

## **Instrumented indentation for determining stress and strain levels of pre-strained DC01 sheets**

Mohamad IDRIS<sup>1\*</sup>, Olivier BARTIER<sup>2</sup>, Dominique GUINES<sup>3</sup>, Lionel LEOTOING<sup>3</sup>, Gérard MAUVOISIN<sup>2</sup>, and Xavier HERNOT<sup>2</sup>

<sup>1</sup>National Research Council Canada, Saguenay, Québec, G7H 8C3, Canada

<sup>2</sup>LGCGM, Université Rennes 1, 3 Rue du Clos Courtel, 35700, Rennes, France

<sup>3</sup>LGCGM, INSA Rennes, 20 Avenue des Buttes de Coëmes, 35708 Rennes, France

### **Abstract**

In classical mechanical testing, determining the stress and strain states of complex shape specimens turns out to be very challenging, especially in the most deformed regions. In the latter case, when not enough material is present, non-destructive testing is needed for determining the corresponding mechanical state. In this study, a novel approach, based on the local quasi-non-destructive instrumented indentation technique (IIT) coupled with the inverse analysis technique (IAT), is used to determine the stress and strain levels of pre-strained DC01 specimens using monotonic and non-monotonic loading paths. Monotonic and cyclic shear tests as well as Marciniak tests, in both plane and equi-biaxial strain states, are used to apply different pre-strain levels. For monotonic loading paths, i.e. monotonic shearing and Marciniak tests, the applied methodology showed very satisfying results in determining the stress and strain states of the pre-strained specimens, especially for pre-strain values close to the representative indentation strain values. A maximum stress error of less than 15% was obtained in the case of the highest applied pre-strain value (29.04%). The purely isotropic Voce hardening law was adopted for determining

the hardening behaviour of the studied specimens in both cases: as-received and pre-strained. In the case of cyclic shear, a mixed isotropic-kinematic hardening law is to be used to determine the stress and strain states of the pre-strained specimens. Adopting a mixed isotropic-kinematic Chaboche hardening law led to satisfying results where the estimation errors of the applied pre-strain value and corresponding yield stress didn't exceed 6% and 1.3%, respectively. The obtained results show that the proposed indentation-based method can be very useful in estimating the work-hardening level and corresponding plastic deformation of pre-strained parts under various loading paths

**Keywords:** Spherical indentation, Shear and Marciniak pre-straining tests, Finite element analysis, Inverse analysis, Metallic materials.

### Nomenclature

- b: Parameter controlling the curvature of the Voce law  
 b': Parameter controlling the curvature of the Voce law in the case of the pre-strained material.  
 CAX4: 4 nodes axisymmetric element  
 DD: Diagonal Direction  
 DIC: Digital Image Correlation  
 E: Young's modulus (GPa)  
 Error<sub>σ</sub>: Relative error between stresses  
 Error<sub>ε</sub>: Relative error between strains  
 ε: Strain  
 $\epsilon_{eq}$ : Equivalent strain calculated based on the Von-Mises criterion  
 $\epsilon_{P0}$ : Applied plastic strain  
 $\epsilon_{P0-applied}$ : Real plastic strain applied on the pre-strained material  
 $\epsilon_{P0-calculated}$ : Calculated plastic strain applied on the pre-strained material  
 γ: Shear strain  
 IAT: Inverse Analysis technique  
 IIT: Instrumented Indentation Technique  
 Q: Maximum expansion of the load surface (MPa)  
 Q': Maximum expansion of the load surface in the case of the pre-strained parameter (MPa).  
 μ: Friction coefficient

- n: Hardening coefficient
- $\nu$ : Poisson's ratio
- R: Radius of the spherical support (mm)
- RD: Rolling Direction
- RoI: Region of Interest
- $\bar{S}$ : Deviatoric stress sensor
- $\sigma$ : Stress (MPa)
- $\sigma_{eq}$ : Equivalent stress calculated based on the Von-Mises criterion (MPa)
- $\sigma_Y$ : Yield strength (MPa)
- $\sigma'_Y$ : Yield strength of the pre-strained material (MPa)
- $\sigma_{Y-reference}$  (MPa);  $Q_{reference}$  (MPa);  $b_{reference}$ : Real Voce parameters for the un-deformed state of the studied material
- $\sigma_{Y-indentation}$  (MPa);  $Q_{indentation}$  (MPa);  $b_{indentation}$ : Calculated Voce parameters for the as-received state of the studied material
- $\sigma'_{Y-reference}$  (MPa);  $Q'_{reference}$  (MPa);  $b'_{reference}$ : Real Voce parameters for the pre-strained state of the studied material
- $\sigma'_{Y-indentation}$  (MPa);  $Q'_{indentation}$  (MPa);  $b'_{indentation}$ : Calculated Voce parameters for the pre-strained state of the studied material
- $\tau$ : Shear stress (MPa)
- TD: Transverse Direction
- X: Kinematic hardening variable

## **1. Introduction**

The instrumented indentation technique (IIT) allows reaching the elastic and plastic properties of a material. With this technique, the elasticity modulus, the hardness, the yield strength, the tensile strength limit, or the strain hardening exponent of a material can be obtained quickly, almost non-destructively, locally, and in situ. Studies and applications carried out on functionally graded materials (FGM) [1] [2], welded steels [3] [4], coated steels [5] [6], composites [7] [8] or polymers [9] [10] have shown that IIT is interesting and reliable for mechanical characterization. The local character of the indentation test and the fact that the test can be performed in situ allow evaluating the mechanical properties during the life cycle of an industrial part or a structure. For example, the effects of irradiation [11], thermal shock [12],

aging in a salty and hot environment [13] and fatigue [14] on the mechanical properties of a material can be evaluated using IIT.

The identification of the mechanical parameters of the indented material is obtained from the post-mortem imprint or/and an F-h curve measured during the indentation test, a curve corresponding to the evolution of the force (F) applied by the indenter according to the displacement (h) of the indenter. To determine the elastoplastic properties of materials from a spherical indentation test, different approaches can be used depending on whether the F-h curve or the imprint is used [2] [3] [15-35]. In almost all the proposed methods, the behaviour law is assumed to be isotropic and an isotropic strain hardening law with less than four unknown parameters is chosen in order to "theoretically" guarantee the uniqueness of the solution [2] [3] [15-18] [22-35]. In the case where the behaviour law of the indented material is anisotropic, the use of a single indentation curve is not sufficient to determine all the many parameters of this law. Recent work has shown that the joint use of the indentation curve and the imprint is a solution to determine the anisotropic plastic properties [36-39]. For many of the proposed approaches, the concept of the representative strain is used to predict the material stress-strain curve [15-21] [23-26] [35] [40] [41]. The advantage of this concept is that it allows obtaining the strain range for which the identified hardening law is the most accurate. The studies performed on the representative deformation in spherical indentation can be divided into two main groups. The first group is based on the use of the F-h curve to reach the mechanical properties of the indented material [15-18] [23-25]. The second group is based on the F-a measured data, where a is the contact radius between the indenter and the indented material deduced from the F-h curve or obtained from the imprint [19-21] [35] [40]. With the use of the F-h curve in spherical indentation, the range of representative strain values is equal to about 0.013-0.045 for Cao and Lu [15], 0.04-0.07 for Zhao et al. [16], and 0.01-0.06 for Moussa et al. [24], depending on h/R

values. When using the imprint or an F-a curve, it has been shown that the representative strains are greater than those obtained from the F-h curve. For Tabor [40], the representative deformation can reach 0.2 if the contact radius is equal to the sphere radius, R. For Jeon et al. [20] and Bartier et al. [41] this representative deformation can reach 18% and 27% respectively when  $a/R=0.8$ . Whatever the approach used, the aforementioned methods consist in optimising the values of the parameters of the work strain hardening law by minimizing the error between the measured experimental data, i.e. F-h curve and/or imprints, and those obtained via an analytical or numerical model [2] [3] [22-34]. Although the inverse analysis leads to optimised values of the strain hardening law parameters, the concept of representative deformation indicates that the hardening law obtained from these optimised parameters is more accurate within a certain range of deformation. Compared to the identification performed from the F-h curve, the representative strains are higher when the inverse analysis is performed from the F-a curve or the imprint, so the strain values for which the identification is most accurate are also higher when the F-a curve or the imprint is used. However, it is important to note that the majority of the studies in this field were based on the F-h curve [2] [3] [15-18] [21-30]. Adopting the F-h curve proves to be relatively simpler and faster, when compared to the other in-situ data extraction approaches.

The plastic pre-strain undergone by a metal leads to a modification of the mechanical properties such as strength, ductility, or fracture toughness. For a metal with isotropic hardening, it is observed that a pre-strain leads to an increase in yield strength and a decrease in ductility. A pre-strain modifies other parameters such as decreasing the toughness and Young modulus of high strength steels [42] [43], hydrogen embrittlement [44], or the hardening or softening of glass, depending on the loading path [45]. Studying the indentation response of as-received and pre-strained materials is one way to evaluate the change in mechanical properties due to pre-

strain [42] [43] [45] [46] [22]. This evaluation can be very useful for determining or anticipating the fracture toughness [42] and the springback of plastically pre-strained sheets [43].

M. Idriss et al. [22] studied the ability of the IIT coupled with the inverse analysis technique (IAT) to determine the strain level of DC01, DP600, and AA2017 metal sheets plastically pre-strained by a monotonic tensile test. In their proposed methodology, the Voce hardening law is considered for describing the mechanical behaviour of the studied materials. The Voce law has the advantage of keeping the same mathematical form after applying a plastic pre-strain. Another advantage is that knowing the hardening law of the as-received material, only one mechanical parameter of the pre-strained material needs to be identified from the IIT and IAT [22]. The results obtained in [22] show that the IIT, coupled with IAT, is very effective in determining the stress levels and plastic strains applied to pseudo-materials and real metal sheets.

In this study, the methodology proposed in [22] is investigated for more complex applications. This includes monotonic and cyclic shear tests as well as Marciniak tests, in the cases of plane and biaxial expansions. For monotonic loading (monotonic shear and Marciniak), the Voce law is adopted where three plastic parameters are determined using IIT coupled to IAT from which the plastic pre-strain is deduced. In the case of cyclic shear, a reverse loading path triggers the Bauschinger effect. Adopting the Voce law is not sufficient for determining correctly the pre-strain of the tested material. This leads to use a more complex hardening law (Chaboche) that takes into account the hardening type (isotropic and/or kinematic). Based on a previous study [47], the contribution of each hardening type is determined. Afterward, the pre-strain value, in the case of cyclic shear, is obtained.

## **2. Methodology**

In [22], the authors presented a method for evaluating the stress and pre-strain levels of plastically pre-strained metal sheets using IIT coupled to IAT (Fig. 1). Pre-strain was applied by

a standard monotonic tensile test. In this study, the same methodology is applied. However, tensile tests are replaced by monotonic and cyclic shear tests as well as Marciniak tests for pre-straining the metal sheets. This is to verify the validity of this methodology in the case of other types of loading paths. The methodology, extensively presented in [22] and summarised in Fig. 2, consists of 4 different steps:

- In step 1, the prepared specimens undergo experimental indentation. The obtained F-h indentation curves are then used in IAT where the 3 parameters of the Voce law, presented in [22], are identified. This is achieved by minimising a cost function between the experimental F-h curve and the numerical indentation curve obtained from the FE model (Fig. 1.a and [22]). A numerical study, detailed in [22] and based on the use of two pseudo-materials following Voce and Hollomon hardening laws, respectively, proved the uniqueness of the obtained solution.
- In step 2, the specimens are pre-strained using different loading paths. Pre-straining is performed using monotonic and cyclic shear tests as well as Marciniak tests. The level of plastic pre-straining and stress ( $\varepsilon_{p0-reference}$  and  $\sigma'_{y-reference}$ ) are then deduced and used as reference values in the last step (4).
- In step 3, the pre-strained specimens are cut, polished, prepared, and indented for obtaining the corresponding F-h indentation curves. The latter curves are then used in IAT for determining the corresponding yield stress of the pre-strained material ( $\sigma'_{y-indentation}$ ). Simplifying conditions determined from IAT in step 1 are considered in the inverse analysis calculation of this step [22].
- In step 4,  $\sigma'_{y-indentation}$  obtained from step 3 is compared to  $\sigma'_{y-reference}$  obtained from step 2. Finally, the calculated plastic pre-strain  $\varepsilon_{p0-indentation}$  is also compared to the applied plastic pre-strain  $\varepsilon_{p0-reference}$  for validating the proposed approach.

## Instrumented Indentation technique (IIT) coupled to Inverse Analysis technique (IAT)

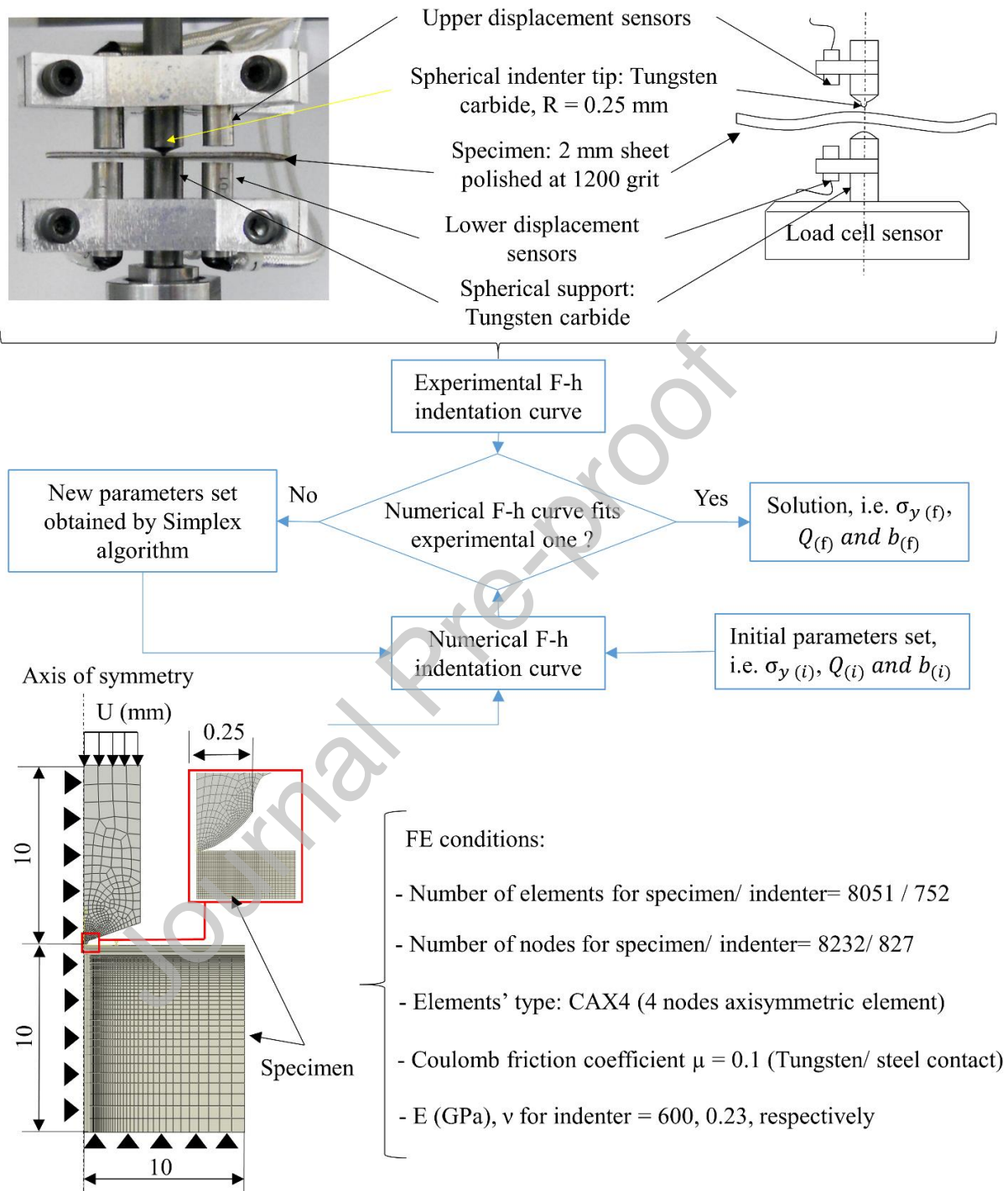


**Fig. 1 Instrumented Indentation Technique (IIT) coupled to the Inverse Analysis Technique (IAT).** The Experimental indentation bench consists of three upper and three lower displacement sensors, thin sheet (specimen), spherical indenter, and load cell sensor. The Numerical FE model represents the indentation test consisting of the spherical indenter tip and a semi-infinite specimen. Correction methods [48] [49] are applied for considering the differences between experimental and numerical conditions. The Inverse analysis technique IAT consisting of minimising the difference between the experimental F-h indentation

curves obtained from the experimental bench and the  $F-h$  numerical ones obtained from the indentation FE model. By minimising the cost function and by respecting the convergence criteria, the three plastic parameters  $\sigma_y$ ,  $Q$ , and  $b$  of the Voce parameters are identified.

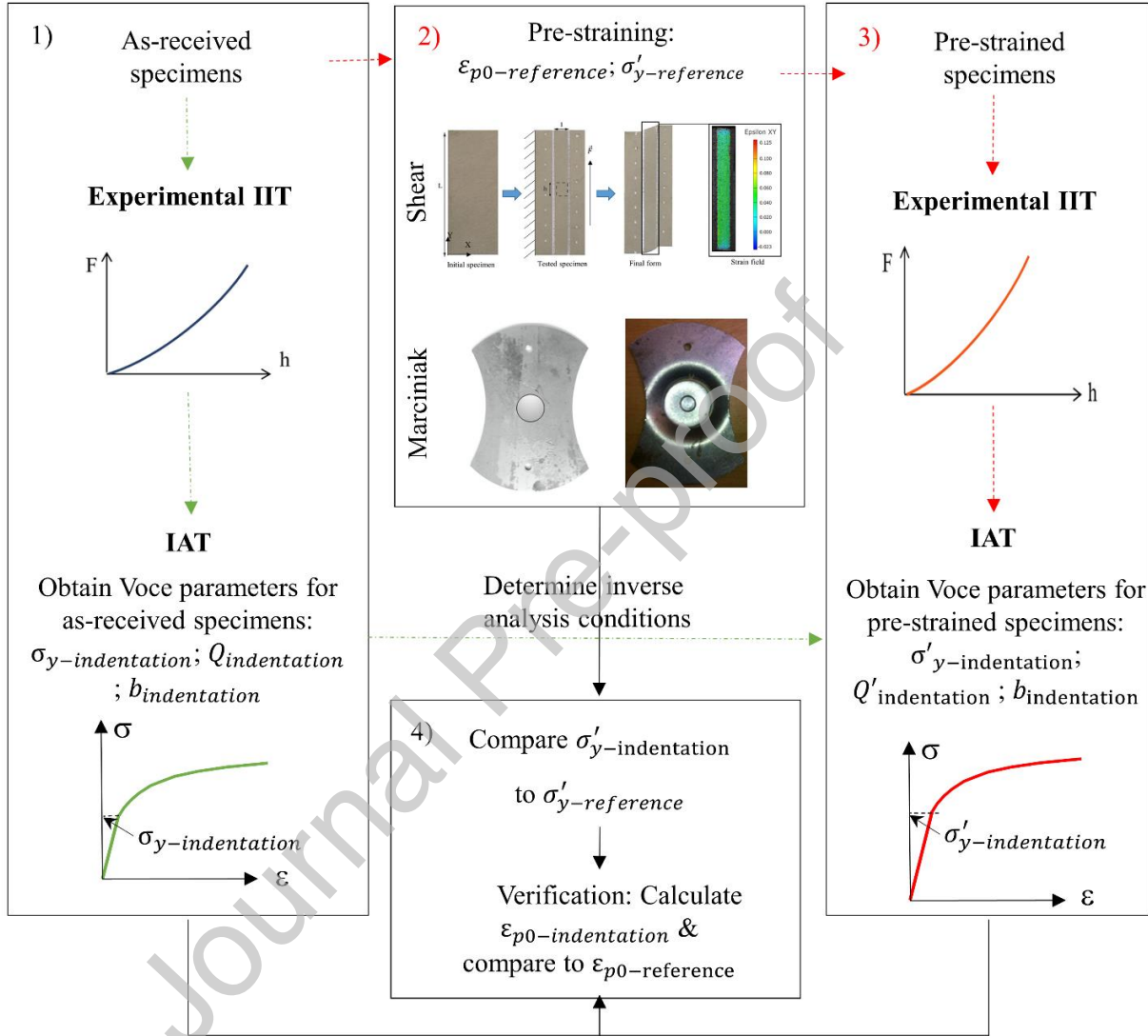


**Fig. 2 Methodology for determining stress and strain levels of pre-stained materials using the IIT coupled to IAT.** Step 1: spherical indentation on as-received specimen and determination of Voce plastic parameters using IAT. Step 2: Pre-straining as-received specimens using monotonic and cyclic shear tests as well as monotonic Marciniak tests: the obtained pre-strains and stresses are noted  $\epsilon_{p0-reference}$  and  $\sigma'_{y-reference}$ , respectively. Step 3: the pre-stained specimens are prepared (cut and polished) for indentation. The specimens are then indented and the obtained  $F-h$  curves are used in IAT to determine the Voce plastic parameters after pre-straining. Step 4: determine  $\sigma'_{y-indentation}$  obtained from step 3 and compare it to  $\sigma'_{y-reference}$  obtained from step 2. For validation of the proposed approach, the calculated plastic pre-strain  $\epsilon_{p0-indentation}$  is also compared to the applied plastic pre-strain  $\epsilon_{p0-reference}$

## 1. Materials and mechanical tests

A 2 mm thick DC01 is investigated in this study. DC01 is an unalloyed cold rolled deep drawing steel. Corresponding chemical composition and microstructure were presented in [22].

### 3.1. *IIT and IAT*

IIT is used to characterise the hardening laws of DC01 in both as-received and pre-strained conditions. All experimental considerations were thoroughly presented in prior studies [22] [47] [50] [51]. The indenter tip is not a perfect sphere. The exact profile of this indenter is measured by Scanning Electronic Microscopy (SEM) and then implemented in the FE analysis (Fig. 1) [48]. As mentioned in section 2, all specimens are cut and polished before indentation. Specimen preparation does not influence the indentation tests. All indentation tests were performed at the center of the specimens. Therefore, the pre-strain levels cannot be influenced by the cut edges. Electrolytic polishing was applied to the specimens. No residual stresses are induced in the specimen's preparation. Within the framework of this study, only shear, plane tensile, and equibiaxial expansion load paths are applied. Therefore, in all these cases, the induced pre-strain is homogeneous through the thickness. Therefore, Using electrolytic polishing for removing relatively thin layers from the surface of the tested specimen does not modify its pre-strain state.

The adopted indentation FE model is a half-space axisymmetric model where the spherical support is not considered (Fig. 1). This is to simplify computations' complexity and time, especially in IAT (Fig. 1). The numerical displacement was extracted at 10 mm from the indenter tip. This corresponds to the exact position of the upper displacement sensors used in the experimental apparatus. Therefore, within the framework of this study, the compliance of the indentation bench is not considered. In addition, correction methods [48] [49] are applied for

considering the differences between experimental and numerical conditions. Corresponding experimental and numerical information is summarised in Fig. 1.

For identifying the plastic parameters of the Voce law, IAT was applied using ModeFrontier software. The adopted minimisation algorithm (Simplex) defines an initial parameters' set ( $\sigma_{y(i)}$ ,  $Q_{(i)}$ , and  $b_{(i)}$ ) that implements in the FE model for obtaining a numerical indentation curve. Then the difference between the obtained numerical curve and the experimental one is calculated using a cost function defined in [52]. Then, the minimisation algorithm tries to decrease the cost function value by determining a new parameters' set ( $\sigma_{y(i+1)}$ ,  $Q_{(i+1)}$ , and  $b_{(i+1)}$ ) to be implemented in the FE model. This process is repeated iteratively until the convergence criterion is reached. The latter is defined as the variation of the cost function value between two consecutive iterations. Whenever this variation drops under  $10^{-8} \text{ N}^2$ , it is considered that the convergence criterion is obtained and that the identified parameter's set is the optimal solution [22] [47] [53]. The identified Voce parameters on the as-received sheets using IIT coupled with IAT are given in Table 1. The corresponding Voce hardening curve is compared to the ones obtained by tensile and shear tests in Fig. 3-d.

**Table 1** Voce plastic parameters obtained for the as-received DC01 using IIT coupled to IAT

	$\sigma_{Y\text{-indentation}}$ (MPa)	$Q_{\text{indentation}}$ (MPa)	$b_{\text{indentation}}$
As-received DC01	208	531	2.39

### 3.2. Tensile and shear tests

Tensile tests were performed following the EN ISO 6892-1 standard [54]. Test conditions and specimens' dimensions were thoroughly presented in [22]. Anisotropy is neglected for the

rest of the study. The corresponding tensile curves obtained in the rolling, diagonal, and transversal directions as well as the corresponding mean tensile curve are recalled in Fig 3-a.

All shear tests were performed in the IRDL at UBS University in France. The corresponding apparatus and methodology were presented in [47] [55]. In this study, shear tests were used to pre-strain the DC01 using two different loading paths: monotonic and cyclic shear (Fig 3-b). The final pre-strain values are approximately the same in both cases (Fig. 3-d and Table 2). From the obtained  $\tau$  (MPa) -  $\gamma$  curves, the equivalent  $\sigma_{eq}(MPa) - \varepsilon_{eq}$  curves are deduced based on the Von-Mises criterion (Fig. 3-d). The final stresses obtained in both cases, corresponding to the total applied plastic pre-strains are summarised in Table 2.

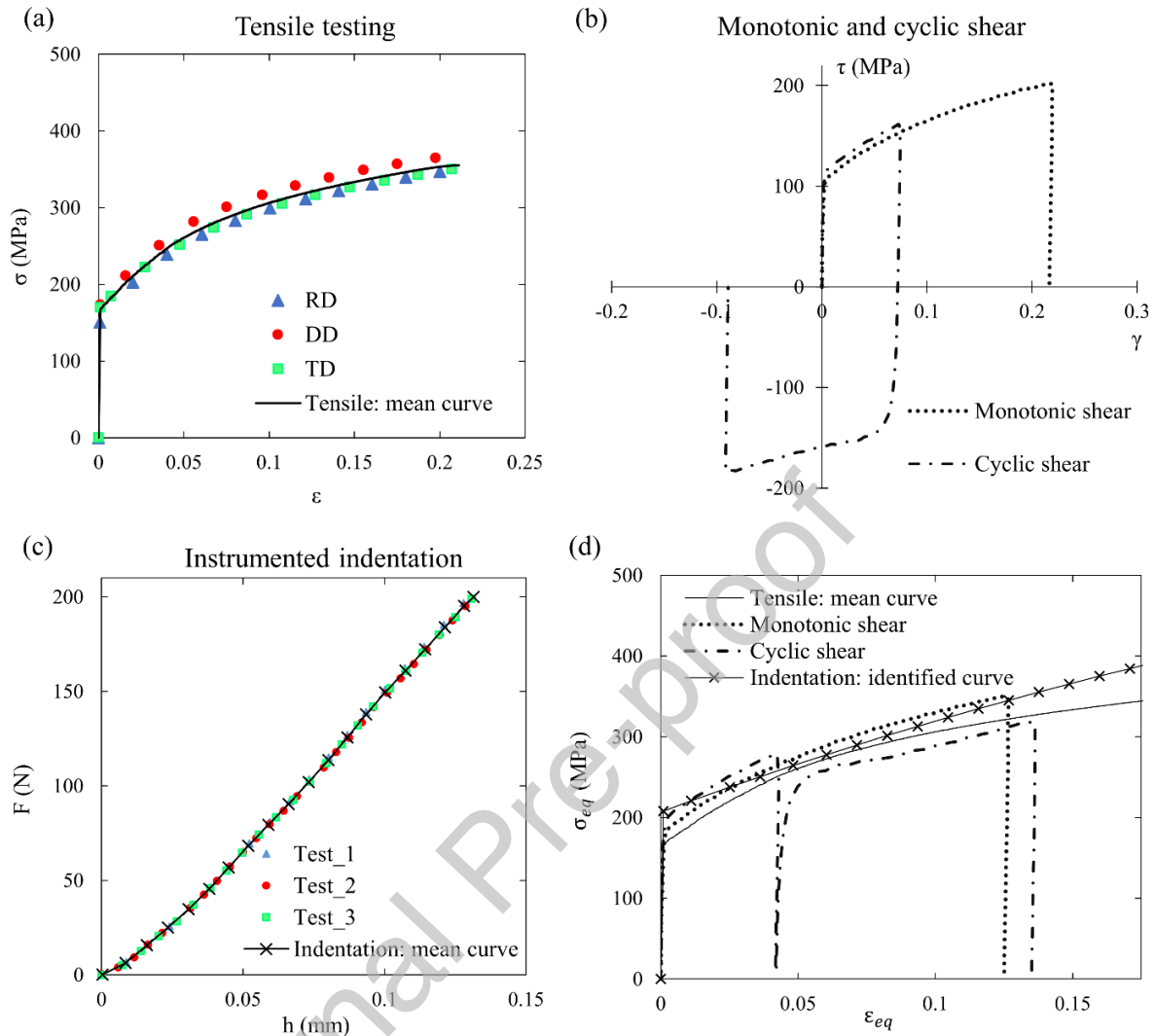


**Fig. 3** DC01 hardening curves obtained from tensile and shear testing as well as DC01 hardening curve identified from  $F$ - $h$  indentation curves (a) tensile curves obtained in the three directions (rolling, diagonal, and transversal) and the corresponding mean curve. (b)  $\tau$  (MPa) –  $\gamma$  shear curves obtained in the case of monotonic and cyclic loading. (c) Three  $F$  (N) –  $h$  (mm) indentation curves obtained on the as-received DC01 specimens and the corresponding mean indentation curve. (d) The tensile mean curve from fig. 3-a, the Von-Mises equivalent cumulative  $\sigma_{eq}$  –  $\epsilon_{eq}$  monotonic and cyclic shear curves from fig. 3-b, and the identified curve based on the indentation-based method (IIT coupled to IAT) from fig. 3-c.

**Table 2** Applied plastic pre-strain  $\epsilon_{p0-reference}$  (%) and corresponding stress level  $\sigma'_{\gamma-reference}$  (MPa) for both loading paths (monotonic and cyclic shear)

Material	Shear path	$\epsilon_{p0-reference}$ (%)	$\sigma'_{\gamma-reference}$ (MPa)
DC01	Monotonic	12.49	350
	Cyclic	13.49	319

### 3.3. Marciniak tests

4 DC01 samples were prepared for the Marciniak test. Two samples undergo plane expansion (specimens PS\_1 and PS\_2) and the remaining two samples undergo biaxial expansion (specimens B\_1 and B\_2). The corresponding specimens' geometrical forms and dimensions are given in Fig. 4. The samples are designed with two different thicknesses. The initial thickness is 2 mm. The thickness of the central zone is 0.8 mm. This thickness reduction is performed for obtaining a strain localization in the central zone.

Grease lubrication is used to reduce friction between the different mechanical parts (punch, sample, and die). Marciniak tests are performed with a servo-hydraulic machine with a maximum loading capacity of 250 kN. The punch speed is about 0.1 mm/s which corresponds to a deformation rate of about  $0.02 \text{ s}^{-1}$ . For both plane and biaxial expansions, low (3.7 and 5 mm) and high (9.7 mm) displacement levels are tested.

To obtain the strain fields, a high-resolution FASTCAM ultima APX-RS digital CMOS camera is used. The images of the surface of the Marciniak sample are recorded at a frequency of 50 Hz as the punch moves. The camera is fixed relative to the punch to avoid out-of-plane motion. The camera focus is set on the surface of the Marciniak sample when it is in contact with the punch. The camera resolution is set to 512 x 512 pixels. The surface displacement field is determined using the Digital Image Correlation (DIC) technique. To improve image contrast, white and black paints were sprayed onto the sample surface prior to testing, resulting in a characteristic speckle pattern of approximately 5 pixels (Fig 4-c). DIC is performed using the GOM2017 software. The region of interest (RoI) used to calculate the displacement field is also represented in Fig 4-c. The corresponding subset size is 22 pixels. The spacing of pixel grid points at which the subset displacements are calculated, called step size, is set to 12 pixels

corresponding to 600  $\mu\text{m}$ . The interpolant is a bi-cubic function. Finally, the tested specimens, applied displacements, and corresponding strains are summarised in Table 3.

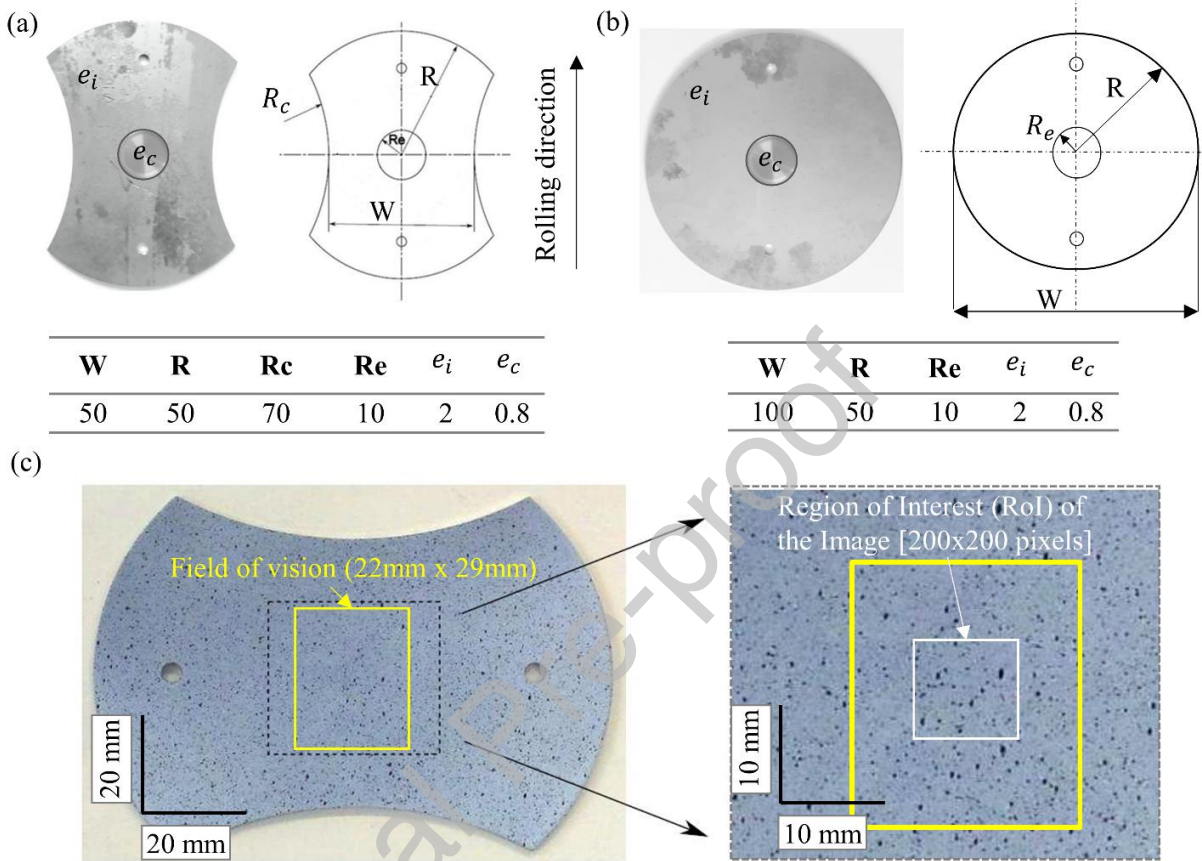


**Fig. 4 Marciniak specimens' forms and dimensions** (a) specimen dimensions in the plane expansion condition:  $R$  being the radius of the tested specimen,  $R_c$  being the radius of the outer curves and  $W$  being the width of the specimen,  $e_i$  being the initial specimen thickness and  $e_c$  being the thickness of the central zone (b) specimen dimensions in the biaxial expansion condition [56]:  $R$  being the radius of the tested specimen and  $R_e$  being the radius of the central zone where thickness reduction is applied for strain localization,  $e_i$  being the initial specimen thickness and  $e_c$  being the thickness of the central zone (c) Black and white speckled sample before Marciniak testing [56]. The yellow rectangle corresponds to the field of vision of the cameras and the white one corresponds to the region of interest (ROI). To note that all dimensions are given in mm.

The average values of major and minor deformation are calculated at 5 points located in a central region of about 3 mm diameter (Figs. 5 and A-1). Considering an incompressible material, these values lead to the principal strains ( $\varepsilon_I$  and  $\varepsilon_{II}$ ) and corresponding cumulative equivalent Von-Mises strain ( $\varepsilon_{eq}$ ) given in equation 1 and shown in Fig. 6.

$$\varepsilon_{eq} = \int d\varepsilon_{eq} \quad \text{with } d\varepsilon_{eq} = \sqrt{\frac{4}{3}(d\varepsilon_I^2 + d\varepsilon_{II}^2 + d\varepsilon_I d\varepsilon_{II})} \quad (\text{eq. 1})$$

From the equivalent strain values obtained by image correlation, the new parameters of the DC01 steel hardening law obtained after Marciniak pre-straining were determined (Table 3). These new parameters were calculated with the following equations [22]:

$$\sigma = \sigma'_Y + Q' \cdot (1 - \exp(-b \cdot (\varepsilon_P))) \quad (\text{eq. 2})$$

$$\text{With: } \sigma'_Y = \sigma_Y + Q - Q \cdot \exp(-b \cdot \varepsilon_{P0})$$

$$Q' = Q \cdot \exp(-b \cdot \varepsilon_{P0})$$

Where  $\sigma_Y$ ,  $Q$  and  $b$  are the Voce's law parameters of the as-received DC01 steel (Table 1) and  $\sigma'_Y$  and  $Q'$  are the Voce's law parameters of the pre-strained DC01 steel with the corresponding plastic pre-strain  $\varepsilon_{P0}$  given in Table 3.

Since the strains measured by image correlation are total strains, and the elastic strains are significantly smaller than the plastic strains in the performed tests, elastic strains will be neglected and the measured cumulative equivalent strains will be assumed to be equal to their plastic part  $\varepsilon_{P0} = \varepsilon_0$ . The Voce law parameters for each Marciniak pre-strained sample obtained from the image correlation technique and (eq. 2) are given in Table 3.

**Table 3** Displacements and corresponding equivalent Von-Mises strains for DC01 specimens pre-strained with Marciniak test: PS\_1: plane strained specimen with small displacement (3.7 mm), PS\_2: plane strained specimen with large displacement (9.7 mm), B\_1: biaxial specimen with small displacement (5 mm), B\_2: biaxial specimen with large displacement (9.7 mm)

Load path	DC01_ Specimen #	Displacement (mm)	$\varepsilon_{\text{Von-Mises}} (\%) = \varepsilon_{P0\text{-reference}} (\%)$	$\sigma'_{Y\text{-reference}}$	$Q'_{\text{reference}}$	$b_{\text{reference}}$
Plane strain	PS_1	3.7	3.75	254	485	2.39
	PS_2	9.7	18	394	345	2.39
Biaxial expansion	B_1	5	5.32	271	468	2.39
	B_2	9.7	29.04	474	265	2.39

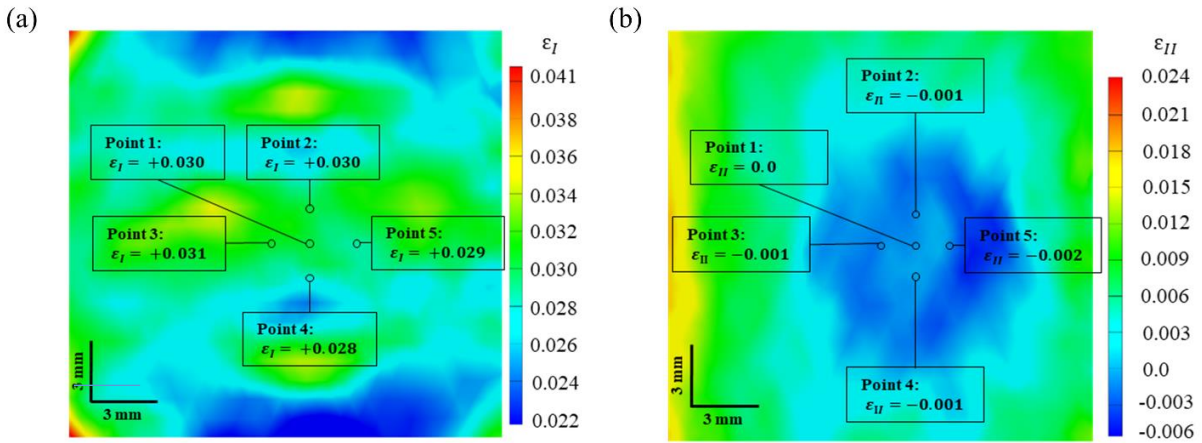


**Fig. 5** Principal strain fields  $\varepsilon_I$  and  $\varepsilon_{II}$  and the corresponding points used for calculating the mean equivalent strains for DC01 specimens undergoing Marciniak tests: (a) PS\_1 (specimen undergoing Marciniak plane strain with a displacement of 3.7 mm):  $\varepsilon_I$ : principal major strain, (b) PS\_1:  $\varepsilon_{II}$ : principal minor strain. The strain fields for the remaining specimens are given in Fig. A-1

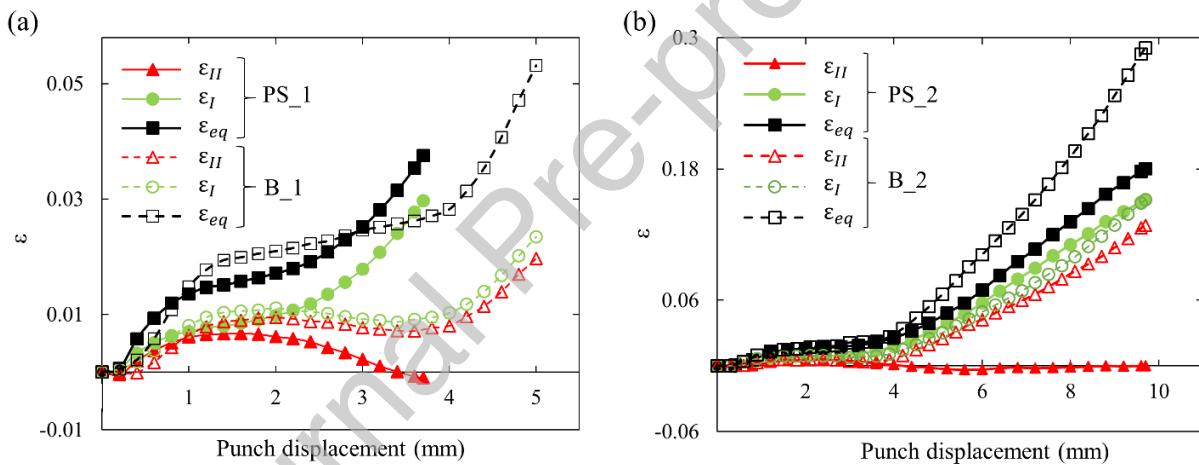


**Fig. 6** Principal ( $\varepsilon_I$  and  $\varepsilon_{II}$ ) and equivalent ( $\varepsilon_{eq}$ ) Von-Mises strains in the case of Marciniak tests obtained from DIC: (a) small displacements (3.7 mm for PS\_1 and 5 mm for B\_1), (b) large displacement (9.7 mm for PS\_2 and B\_2)

## 4. Results and discussion

### 4.1. Indentation of as-received and pre-strained specimens

#### 4.1.1. Indentation of monotonic and cyclic sheared specimens

The obtained shear specimens were cut and mirror-polished for the indentation tests (Fig 7-a). The same indentation conditions used in the identification of the as-received specimens were adopted for the indentation of the sheared samples: this includes the adopted indenter, the

maximum applied force (200 N), the indentation speed (2 $\mu$ m/s), and reproducibility tests (minimum of three tests). The obtained mean loading curve from each pre-straining condition was then used in the IAT (Fig. 7-a).

From Fig. 3-d, the specimens that underwent cyclic shearing are less resistant than specimens with monotonic shear pre-straining. This is in full agreement with Fig. 7-a where, for the same equivalent plastic pre-strain, the obtained strength is less in the case of cyclic shearing. This is mainly due to the Bauschinger effect that occurs in the case of non-monotonic loading paths [47].

#### 4.1.2. Indentation of Marciniak pre-strained specimens

The strain fields located in a central zone of 3 mm diameter are relatively homogeneous (Fig. 5). Therefore, all four specimens, pre-strained using Marciniak tests, were then cut, mirror-polished, and then, indented in the identified central zone. The obtained indentation curves of the tested samples as well as the indentation curve of the as-received DC01 are presented in Fig. 7-b. The obtained F-h curves correspond well to the applied Marciniak strain levels: for example, specimen B\_2, corresponding to the highest pre-strain value (29.4 %), has also the highest resistance indentation curve.

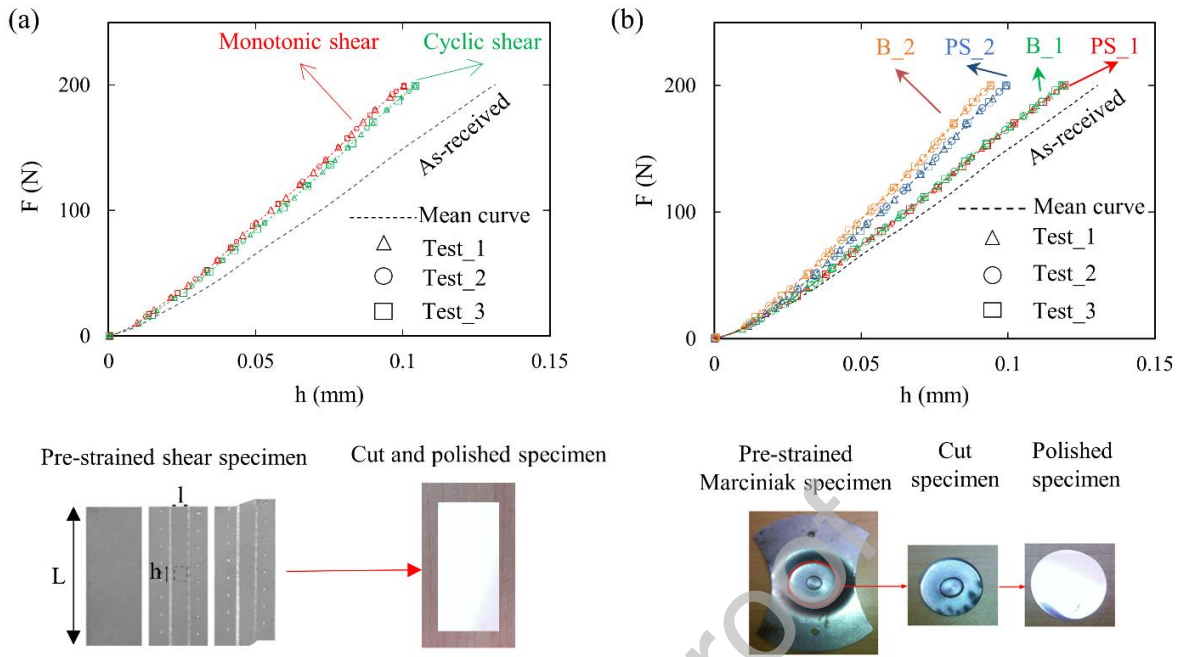


**Fig. 7 (a)**  $F$  (N) –  $h$  (mm) indentation curves before and after pre-straining by monotonic and cyclic shearing and corresponding specimens' preparation. Results are in agreement with what was obtained in Fig. 3-d where for approximately the same pre-strain level, monotonic shearing led to a cumulative stress value higher than the one obtained in the case of cyclic shearing (b)  $F$  (N) –  $h$  (mm) indentation curves obtained for as-received and Marciniak pre-strained specimens and corresponding specimens' preparation. Results are in agreement with the values presented in Table 3 and Fig. 6 where for PS\_1 and B\_1 (small displacements), the corresponding indentation curves show less resistance than the ones obtained for PS\_2 and B\_2 (large displacements)

## 4.2. Monotonic pre-strained specimens

### 4.2.1. Results for monotonic shearing and Marciniak loading paths

Specimens pre-strained with monotonic loading paths are studied together. This includes specimens with monotonic pre-strain shear as well as specimens with Marciniak pre-straining (plane and bi-axial expansions).

The indentation curves, obtained on the pre-strained samples, are used in IAT to determine Voce's plastic parameters considering the conditions proposed in the methodology presented in [22]. In the following, the main conditions imposed in the inverse analysis calculation are recalled:

$$\sigma'_Y + Q' = \sigma_Y + Q = 208 + 531 = 739 \quad (\text{eq. 3})$$

Where  $\sigma_Y$  (MPa) and  $Q$  (MPa) are the yield strength and maximum surface load expansion before pre-straining, respectively and  $\sigma'_Y$  (MPa) and  $Q'$  (MPa) are the yield strength and maximum surface load expansion after pre-straining, respectively.

The hardening parameters ( $\sigma'_{Y-indentation}$ ,  $Q'_{indentation}$ , and  $b_{indentation}$ ), obtained from IAT for the specimens sheared monotonically and pre-strained in plane and biaxial expansions, are presented in Table 4. The real pre-strain yield stresses  $\sigma'_{Y-reference}$ , presented in Tables 2 & 3, are recalled in Table 4. The error % (Error <sub>$\sigma$</sub> ) between  $\sigma'_{Y-indentation}$  and  $\sigma'_{Y-reference}$  is also calculated for each case (Fig. 8).

From the obtained hardening parameters, the plastic pre-strain is calculated  $\varepsilon_{p0-indentation}$  using (eq. 4) based on IAT and the aforementioned methodology [22].

$$\varepsilon_{p0-indentation} = \frac{-1}{b_{indentation}} \ln \frac{Q'_{indentation}}{Q_{indentation}} \quad (\text{eq. 4})$$

The plastic pre-strain calculated from IIT coupled to IAT  $\varepsilon_{p0-indentation}$  is compared to the real plastic pre-strain  $\varepsilon_{p0-reference}$  (Table 4). The corresponding error is presented in Fig. 8. From Table 4 and Fig. 8, the presented methodology leads to very satisfying results regarding the determination of the yield strength reached by the pre-strained material independently of the monotonic loading path followed. In the case of pre-strain applied by tensile test, it has been shown that the error on the yield strength of the pre-strained materials does not exceed 2% [22]. For specimens pre-strained with monotonic shear, stress errors were less than 1%. In the case of plane and biaxial expansions, stress errors didn't exceed 15%. Finally, for the highest pre-strain values (PS\_2 and B\_2), an acceptable underestimation of the yield strengths was obtained.

Concerning plastic pre-strains, higher error values are obtained when compared to the ones obtained in the case of yield stresses (Fig. 8). This is mainly observed in the case of Marciniak tests (plane and biaxial expansions). This is related to the DC01 material that is weakly work-hardened ( $Q = 513$  MPa (Table 1)). This leads to a flattened hardening curve where a small error on stress estimation leads to a relatively high error on strain estimation.

**Table 4** Voce's hardening parameters and plastic pre-strains calculated from the proposed methodology for the different monotonically pre-strained specimens, applied yield strengths, and plastic pre-strains

Load path	Displacement (mm)	$Q'_{indentation}$ (MPa)	$b_{indentation}$	$\sigma'_{Y-indentation}$ (MPa)	$\sigma'_{Y-reference}$ (MPa)	$\epsilon_{p0-reference}$ (%)	$\epsilon_{p0-indentation}$ (%)
Monotonic shear	/	386	2.39	353	350	12.5	13.29
Marciniak _ plane expansion	3.7 (PS_1)	478	2.39	260	254	3.75	4.35
	9.7 (PS_2)	385	2.39	354	394	18	13.4
Marciniak _ biaxial expansion	5 (B_1)	481	2.39	254	271	5.32	4.1
	9.7 (B_2)	336	2.39	403	474	29.04	19.16
Monotonic tensile [22]	5	492	2.39	247	248	3.32	3.15
	9	450	2.39	289	283	6.58	6.9
	18	405	2.39	334	341	13.9	11.35

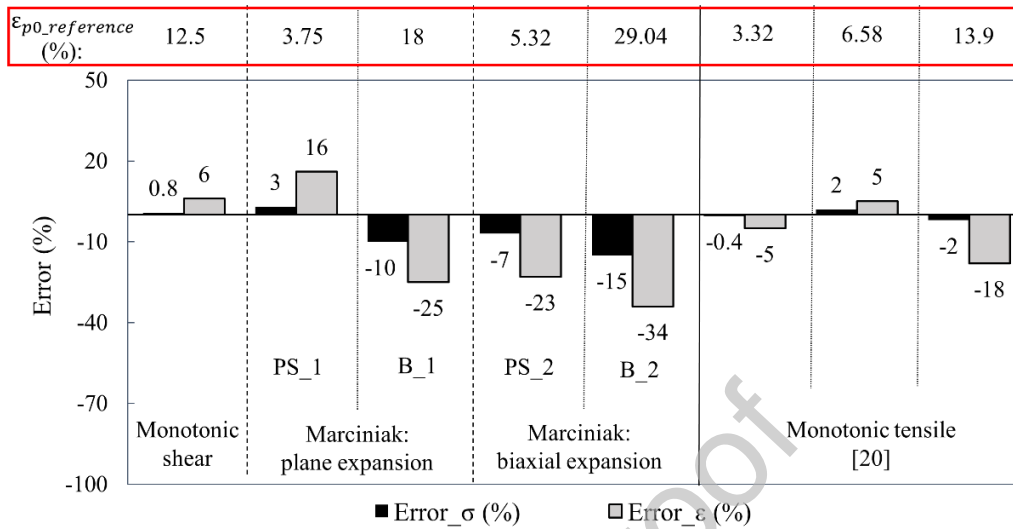


**Fig. 8** Error\_σ: error % calculated between  $\sigma'_{Y-indentation}$  and  $\sigma_{Y-reference}$ , Error\_ε: error % calculated between  $\varepsilon_{p0-reference}$  (%) and  $\varepsilon_{p0-indentation}$  (%). These errors are calculated and represented in the case of monotonic shear, Marciniak plane expansion, and Marciniak biaxial expansion. The errors are also recalled from [22] for the case of monotonic tensile testing.  $\varepsilon_{p0-reference}$  (%) (applied pre-strain) is also represented for each case.

#### 4.2.2. Discussion concerning Marciniak tests: plane and biaxial expansions

For plane and biaxial expansions, a small underestimation of stresses, leading to an underestimation of pre-strains, is generally obtained. This is mainly related to the Voce law adopted for identifying the hardening curve of the studied material. Fig. 9 presents the comparison between the Voce hardening law obtained using indentation and the tensile curves for the as-received DC01. The Voce-type hardening curve, identified from the indentation test, is the closest to the DC01 tensile curves for strain values less than 15% (Fig. 9). This is in agreement with previous studies that presented and analysed the concept of the representative strain of the spherical indentation test [24] [23]. The indentation representative strain is generally between 3% and 6%. It is therefore for this strain range that indentation identification is the most accurate.

For pre-strain levels above 15%, the identification by indentation performed on the as-received DC01 steel leads to a strain hardening curve above those obtained by tensile testing (Fig. 9). For these pre-strain levels, when the mean curve is adopted, the same stress load leads to a higher pre-strain value than the one obtained when the Voce curve, identified by indentation, is adopted. For example, in the case of the PS\_2 specimen that underwent large displacement (9.7 mm) plane expansion, the yield strength identified using indentation is 353 MPa (Table 4). This corresponds to a 13.4 % pre-strain value if the Voce curve, identified by indentation, is adopted. This same yield strength leads to a 17.6% pre-strain value if the mean tensile curve is considered (Fig. 9) which is approximately equal to the applied pre-strain (18 %) (Table 4). In the case of the B\_2 specimen that underwent large displacement (9.7 mm) biaxial expansion, the yield strength identified using indentation is 403 MPa (Table 4). This corresponds to a 19.2 % pre-strain value if the Voce curve, identified by indentation, is adopted. This same yield strength leads to a 32.5% pre-strain value if the mean tensile curve is considered (Fig. 9) which is approximately equal to the applied pre-strain (29.04 %) (Table 4).

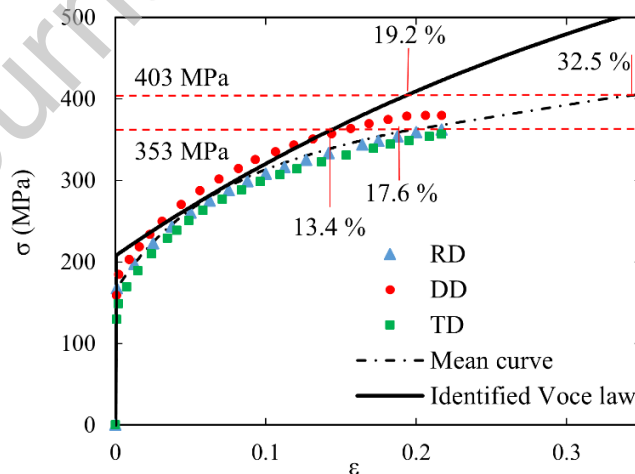


**Fig. 9** Stress-strain curves obtained from tensile testing on as-received DC01 from specimens cut in three different directions: RD, DD, and TD. In addition, the tensile mean curve is represented as well as the identified Voce curve obtained from IIT coupled to IAT. 353 MPa and 403 MPa are the yield stresses identified using IAT for specimens PS\_2 and B\_2 (specimens undergoing large displacements: 9.7 mm). From the identified yield stresses, the real and identified plastic pre-strains are deduced. For B\_2 (403 MPa), 19.2 % pre-strain is obtained instead of 32.5 %. For PS\_2 (353 MPa), 13.4 % pre-strain is obtained instead of 17.6 %.

#### 4.2.3. Discussion concerning monotonic shearing

The proposed methodology allows to determine reliably the pre-strain level undergone by monotonically sheared DC01 sheets (errors less than 6%, Fig. 8). In Fig. 10, the experimental curve obtained from the monotonic shear test is compared to the one identified using spherical indentation. The corresponding parameters for the latter curves were presented in Table 1. These parameters allow reproducing, relatively correctly, the monotonic shear behaviour of the as-received steel sheet.

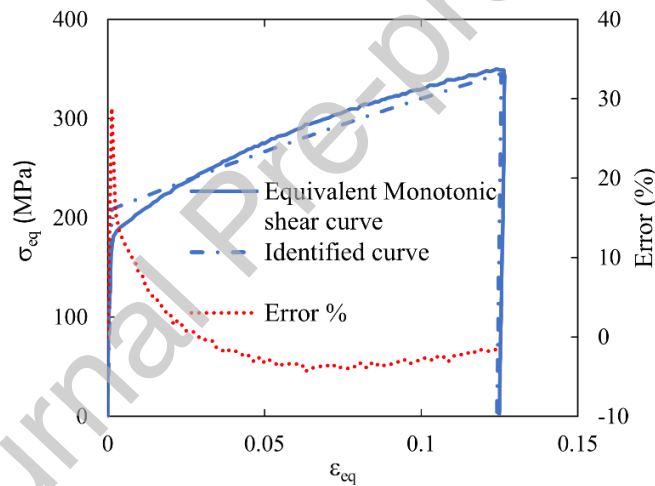


**Fig. 10** Equivalent stress-strain  $\sigma_{eq}$  (MPa) –  $\varepsilon_{eq}$  monotonic shear curves calculated based on the Von-Mises criteria: experimental shear curve and numerical shear curve plotted based on the Voce parameters identified using IIT coupled to IAT. The error % between the experimental shear curve and the identified one is also plotted (secondary y-axis)

For strain values between 0 and 15 %, identification by indentation leads to hardening laws relatively close to those obtained by classical tensile or shear tests (Fig. 3). For the tested material, the identified Voce law leads to an equivalent Von-Mises stress of 345 MPa for the total applied plastic pre-strain ( $\varepsilon_{eq} = 12.49$  %). This stress value is approximately equal to the yield stress identified by indenting the pre-strained DC01 sheet (353 MPa from Table 4). Both

values are also very close to the real stress obtained directly from the shear tests (350 MPa). These results show the validity of the overall methodology for determining the stress and strain states of sheets pre-stained following a monotonic loading path, especially when the hardening law, identified by indenting the as-received sheet, faithfully follows the real hardening law of the tested material.

#### 4.3. Cyclic shear pre-strained specimens

##### 4.3.1. Results for cyclic shear loading path

For an equivalent strain level, the indentation curves obtained for the cyclic shear specimens are located to the right of the indentation curves obtained from the monotonic sheared specimens (Fig. 7-b). This indicates that, for a similar strain level, the cyclic sheared materials are less resistant than the monotonic sheared materials. This is confirmed by the obtained shear curves (Fig. 3-d). By running the inverse analysis calculations and adopting the same conditions used in the case of the as-received and monotonic sheared specimens, the work hardening parameters of the cyclic sheared specimens are determined (Table 5).

**Table 5** Identified Voce parameters for cyclic shear specimens identified using the proposed methodology

Load path	$Q'_{indentation}$ (MPa)	$b_{indentation}$	$\sigma'_{Y-indentation}$ (MPa)	$\sigma'_{Y-reference}$ (MPa)	Error_σ (%)
Cyclic shear	416	2.39	323	319	1.3

From Table 5, the calculated yield stresses for cyclic sheared specimens are lower than the ones obtained from monotonic sheared specimens (353 MPa from Table 4). Moreover, for equivalent strain levels, the obtained stresses are lower in the case of cyclic shearing than the ones obtained in the case of monotonic shearing (Fig. 3-d). This is due to the Bauschinger effect that is triggered in the case of non-monotonic loading paths indicating the presence of a kinematic hardening component in the overall hardening law of DC01. In previous works, cyclic

shear tests and cyclic indentation tests were conducted on the same studied material [47] [53]. In these studies, Chaboche's one-term kinematic hardening law (eq. 5) was adopted to examine the work hardening type of the material:

$$\sigma = \sigma_Y + Q(1 - \exp(-b\varepsilon_p)) + \frac{C}{\gamma}(1 - \exp(-\gamma\varepsilon_p)) \quad (\text{eq. 5})$$

Using Von-Mises plasticity criteria:

$$\sigma_{Von\ Mises} = \sigma_{eq} = \sqrt{\frac{3}{2}} \|\bar{S} - X\| \leq \sigma_Y + R \quad (\text{eq. 6})$$

with  $R = Q(1 - \exp(-b\varepsilon_p))$  and  $dX = Cd\varepsilon_p - \gamma X|d\varepsilon_p|$

In eq. 6, Scalar variable R describes the increase of the elastic domain (expansion of the load surface in the deviatoric space), the tensor variable X describes the displacement of the center of the elastic domain in the deviatoric space and  $\bar{S}$  is the deviatoric stress tensor. To study the influence of each hardening type, the assumption  $b=\gamma$  is considered, which allows the same evolution of both hardening types as a function of strain.

M. Idriss et al. [47] [53] showed that kinematic hardening has a significant influence on the unloading-reloading indentation curve (hysteresis loop). Based on hysteresis loops, they proposed a new approach for determining the influence of each hardening type (isotropic or kinematic) on the overall hardening law of the tested material. The proposed approach was validated by comparing the results obtained with the results obtained from cyclic shear tests [47]. Their studies showed that the percentage of contribution of kinematic hardening is 46% for DC01 [53]. This result shows that the work hardening of DC01 steel is less kinematic than that of DP600 steel studied in [47], which is in agreement with the results found by Sylvestre et al. [57]. Their study showed that isotropic hardening was predominant in the case of DC01 steel. The isotropic or kinematic character of metals is related to their microstructural composition. According to Sylvester et al. [57], ferritic materials show a tendency towards isotropic behaviour

and are not significantly affected by the Bauschinger effect. DC01 steel is composed of a predominantly ferritic microstructure which explains the rather isotropic character of its work hardening behaviour. This is not the case with, for example, dual-phase steels. The existence of two phases at different strengths, hard martensite, and soft ferrite, leads to a non-linear development of internal stresses distributed non-uniformly between these two phases. This leads to inhomogeneous plastic flow in these two phases [58] [59]. This variation in the deformation mechanism between the phases causes a more important Bauschinger effect and thus the highly kinematic behaviour of dual phase steels [57] [58] [59] [60]. Considering that the percentage of kinematic hardening is 46% for DC01, the parameters of the Chaboche hardening law with one kinematic strain hardening term are deduced from the indentation and/or shear tests (Table 6). From the identified parameters in Table 6, cyclic shear numerical simulations were conducted on a one-element C3D8R model using the Abaqus software. The obtained numerical curves are compared to the experimental ones in Fig. 11. The obtained numerical curves do not represent perfectly the Bauschinger effect. However, they estimated correctly the stress values reached at the end of the shear cycles. From Fig. 11-a, the evolution of the corresponding Von-Mises stresses as a function of the equivalent strains is obtained for each steel (Fig. 11-b). Finally, the plastic pre-strains obtained from the presented indentation methodology are compared to the plastic pre-strains applied through cyclic shearing (Table 7).

**Table 6** Identified Chaboche parameters for as-received DC01 sheets [47] [53]

	$\sigma_y$ (MPa)	$Q$ (MPa)	$b$	$C$ (MPa)	$\gamma$
As-received DC01	208	287	2.39	584	2.39

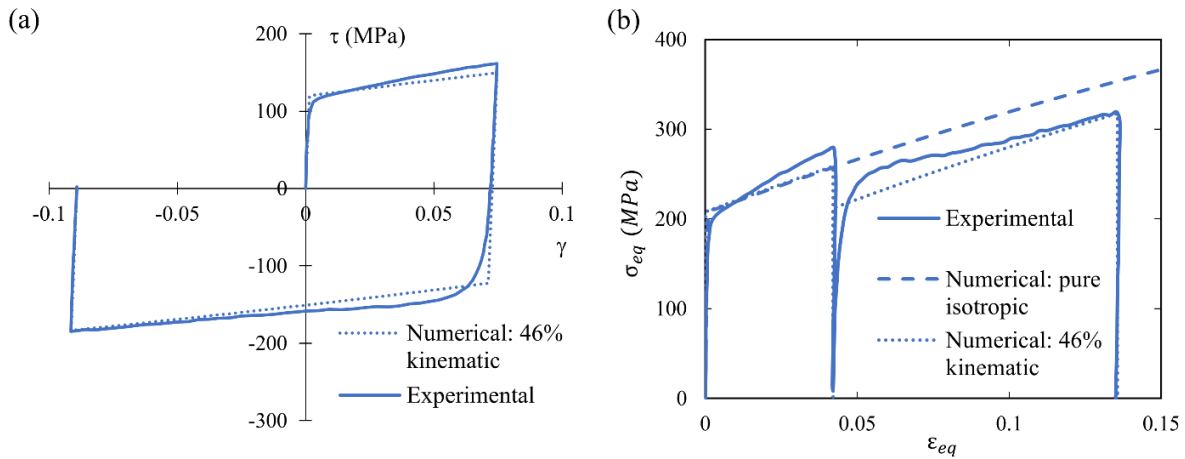


**Fig. 11** Experimental and numerical curves obtained in the case of cyclic shearing (a) experimental  $\tau$  (MPa) –  $\gamma$  shear curve and numerical cyclic shear curve obtained by considering a 46% contribution of kinematic hardening (b) Equivalent Von-Mises stresses (MPa) to equivalent strains for as-received DC01 for three cases: experimental, numerical considering pure isotropic hardening, and numerical considering mixed hardening: 46% of kinematic hardening, i.e. isotropic hardening of 54%

**Table 7** Calculated plastic pre-strains compared to the plastic pre-strains applied through cyclic shearing and the corresponding error between the two pre-strains

	$\epsilon_{p0}$ –reference (%)	$\epsilon_{p0}$ –indentation (%)	Error_ε (%)
Cyclic shear (Chaboche)	13.49	14.2	5.26

#### 4.3.2. Discussion concerning cyclic shearing

The obtained Voce parameters from indentation permitted identifying a Chaboche plastic law with one kinematic component (Table 6). The identified law reproduced relatively correctly the cyclic shear behaviour of DC01 for the studied strain levels.

From literature, the Bauschinger effect is generally attributed to long-range effects, such as internal stresses due to dislocation interactions, dislocation stacking at grain boundaries or Orowan loops around strong precipitates, as well as short-range effects, such as the orientation of mobile dislocations with respect to their motion resistance or the dislocations' annihilation during reverse loading [57] [61] [62] [63] [64]. The Bauschinger effect consists of two mechanisms: the transient softening phase followed by the permanent softening phase. The Bauschinger transient strain is composed of an early re-plasticization and a smooth elastic-plastic

transition with a rapid change of the strain hardening rate. The early re-plasticization and the part of this zone of high curvature of the second loading curve is due to the encounter of dislocations with obstacles easier to cross during the reversal of loading, to the annihilation of dislocations of opposite signs, and also to the microscopic restoring stresses generated by the previously accumulated dislocations which help the movement of the dislocations in the reverse loading direction. The permanent softening phase with its first stage of strain hardening stagnation is a consequence of the phenomena produced in the first phase. In this phase, the stagnation of hardening can be explained by the partial disintegration of the realized dislocation cell structures and the subsequent resumption of work hardening to the formation of new dislocation structures.

Fig. 11 shows an early re-plasticization and stagnation of the strain hardening of DC01 steel after the load reversal over the studied strain range. Although the adopted Chaboche law does not perfectly reproduce the transient phase of the Bauschinger effect, the Von-Mises stress calculated using this law at the end of cyclic shearing is quite close to that obtained experimentally. Fig. 11-a shows that the cyclic shearing of the DC01 steel carried out up to an equivalent Von-Mises plastic strain of 13.49% leads to a 318 MPa Von-Mises stress obtained numerically. This stress, obtained numerically from the law identified by indenting the as-received DC01 steel, is very close to the yield strength identified by indenting the pre-strained specimen (323 MPa, Table 5). It is also very close to the equivalent stress calculated directly from the shear tests (319 MPa, Figs 3-c and 11-a). Based on the evolution of the Von-Mises stress obtained numerically from the parameters of Chaboche's law identified by indenting the as-received sheet (Table 6), the yield strength identified experimentally by indentation of the pre-strained sheet, i.e.  $\sigma'_{y-indentation} = 323 \text{ MPa}$ , leads to an equivalent strain,  $\varepsilon_{p0-indentation}$ , of 14.2% (Table 7). This result shows that considering the hardening type leads to a plastic

equivalent strain of the pre-strained sheet relatively close to the one measured experimentally ( $\varepsilon_{p0-reference} = 13.49\%$ , Tables 2 and 7). This result shows the validity of the indentation test to estimate the hardening level obtained after a mechanical test. This is especially true when the hardening law, previously identified by indenting the as-received sheet, follows faithfully the reference hardening law of the studied material.

Journal Pre-proof

## **5. Conclusions**

In this study, the ability of the instrumented indentation technique coupled with the inverse analysis technique to determine the stress and strain levels of pre-strained materials is investigated. Monotonic and cyclic shearing as well as Marciniak tests, in both plane and biaxial expansion cases, were used for pre-straining the studied specimens. A deep drawable DC01 steel with 2 mm thickness is investigated.

The applied methodology showed very satisfying results in predicting the stress and strain levels of the pre-strained specimens in the case of shearing. For monotonic shearing, the applied stress and strain levels were identified exactly and a corresponding stress error of  $< 1\%$  was obtained. For cyclic shear, the yield stress of the pre-strained material was obtained with an error of less than 1.3%. Taking into account kinematic hardening, the error on the pre-strain estimation didn't exceed 6%. For Marciniak tests, DC01 specimens were studied under two loading types: plane and biaxial expansions. For both cases, two displacement levels were applied: low (3.7 mm for plane expansion and 5 mm for biaxial expansion) and high (9.7 mm for both loading types). For all the tested configurations, the applied methodology showed very satisfying results, especially in the case of stress evaluation where a maximum stress error of  $< 15\%$  was obtained. For strain estimation, less satisfying results were obtained especially for high pre-strain values. An underestimation of 34% was obtained for the highest pre-strain applied. This is mainly due to the identified purely isotropic hardening Voce law that deviates from the standard tensile curves for strain levels  $> 15\%$ . This can be improved by including the  $F-a$  ( $a$  being the contact radius) indentation curve in addition to the  $F-h$  curve. This achieves higher representative strains and, therefore, better accuracy for the high pre-strain values.

## **Declaration of interest statement**

**a. Conflicts of interest/Competing interests**

The authors have no relevant financial or non-financial interests to disclose.

**b. Consent for publication**

The authors confirm that the article is original and that none of the material in the submitted manuscript is currently under consideration for publication elsewhere or has been published previously. All the authors listed on the manuscript have seen and approved the submission of this version of the manuscript and take full responsibility for the manuscript. The authors disclose that there are no prior publications or submissions with any overlapping information. This manuscript has not been and will not be submitted to any other journal while it is under consideration by *the 'International Journal of Mechanical Sciences'* journal.

**c. Funding**

The author(s) disclosed receipt of the following financial support for the research, authorship, and/or publication of this article: This work was supported by 'ESI-group', 'la Région Bretagne', and 'Rennes métropole'.

**d. Availability of data and material (data transparency)**

Due to the nature of this research directly related to confidential industrial applications, participants of this study did not agree for their data to be shared publicly, so supporting data is not available.

**e. Ethics approval**

This article does not contain any studies with human participants or animals performed by any of the authors.

**Declaration of Competing Interest**

None.

**Acknowledgment**

This work has been financially supported by “ESI-Group”, “la Région Bretagne” and “Rennes métropole”.

Journal Pre-proof

## Appendix A:

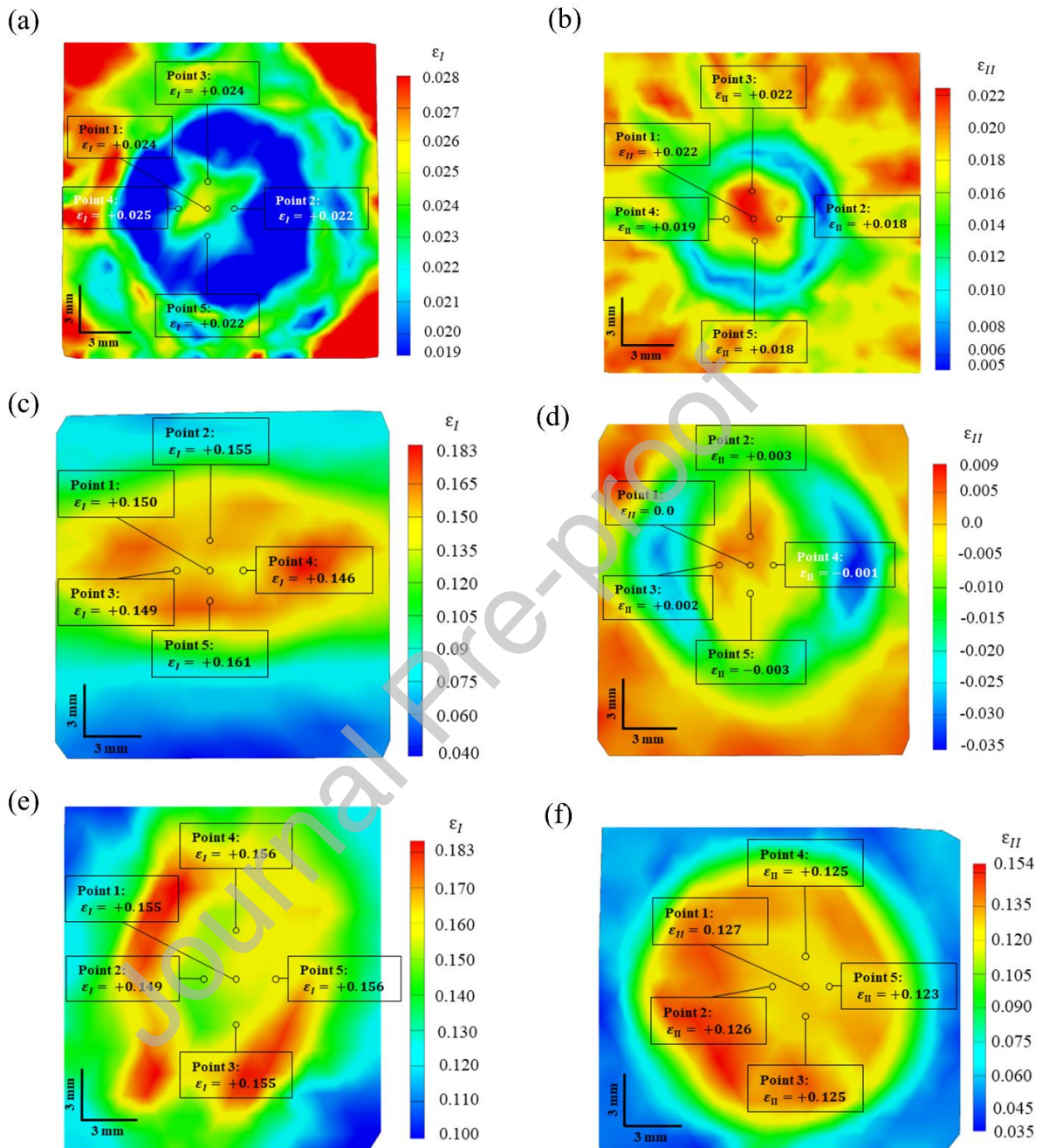


**Fig. A-1** Principal strain fields  $\epsilon_I$  and  $\epsilon_{II}$  and the corresponding points used for calculating the mean equivalent strains for DC01 specimens undergoing Marciniaik tests: (a)  $B_1$ :  $\epsilon_I$ , (b)  $B_1$ :  $\epsilon_{II}$ , (c)  $PS_2$ :  $\epsilon_I$ , (d)  $PS_2$ :  $\epsilon_{II}$ , (e)  $B_2$ :  $\epsilon_I$ , (f)  $B_2$ :  $\epsilon_{II}$ .

## References

- [1] M. Zhao, X. Han, G. Wang, and G. Xu, "Determination of the mechanical properties of surface-modified layer of 18CrNiMo7-6 steel alloys after carburizing heat treatment," *International Journal of Mechanical Sciences*, vol. 148, pp. 84–93, 2018.
- [2] C. Moussa, O. Bartier, G. Mauvoisin, X. Hernot, J.-M. Collin, and G. Delattre, "Experimental and numerical investigation on carbonitrided steel characterization with spherical indentation," *Surface and Coatings Technology*, vol. 258, pp. 782–789, 2014.
- [3] J. J. Kim, T.-H. Pham, and S.-E. Kim, "Instrumented indentation testing and FE analysis for investigation of mechanical properties in structural steel weld zone," *International Journal of Mechanical Sciences*, vol. 103, pp. 265–274, 2015.
- [4] S. Nagaraju, J. GaneshKumar, P. Vasantharaja, M. Vasudevan, and K. Laha, "Evaluation of strength property variations across 9Cr-1Mo steel weld joints using automated ball indentation (ABI) technique," *Materials Science and Engineering: A*, vol. 695, pp. 199–210, 2017.
- [5] N. K. Fukumasu and R. M. Souza, "Numerical evaluation of cohesive and adhesive failure modes during the indentation of coated systems with compliant substrates," *Surface and Coatings Technology*, vol. 260, pp. 266–271, 2014.
- [6] D. Chicot *et al.*, "A contact area function for Berkovich nanoindentation: Application to hardness determination of a TiHfCN thin film," *Thin Solid Films*, vol. 558, pp. 259–266, 2014.
- [7] N. Zhao *et al.*, "Hardness and yield strength of micro-nano TaC-Fe composite layer characterized through nano-indentation, finite element simulation and dimensional analysis," *Ceramics International*, vol. 46, no. 3, pp. 3479–3489, 2020.
- [8] Q. Q. Huang *et al.*, "Spherical indentation with multiple partial unloading for assessing the mechanical properties of ZrB<sub>2</sub>-SiC composites," *Ceramics International*, vol. 41, no. 9, pp. 12349–12354, 2015.
- [9] L. Rabemananjara, X. Hernot, G. Mauvoisin, A. Gavrus, and J.-M. Collin, "Formulation of a representative plastic strain and representative plastic strain rate by using a conical indentation on a rigid visco-plastic material," *Materials & Design*, vol. 68, pp. 207–214, 2015.
- [10] G. Kermouche, J. L. Loubet, and J. M. Bergheau, "Extraction of stress-strain curves of elastic-viscoplastic solids using conical/pyramidal indentation testing with application to polymers," *Mechanics of Materials*, vol. 40, no. 4–5, pp. 271–283, 2008.
- [11] X. Xiao, S. Li, and L. Yu, "Effect of irradiation damage and indenter radius on pop-in and indentation stress-strain relations: Crystal plasticity finite element simulation," *International Journal of Mechanical Sciences*, vol. 199, p. 106430, 2021.
- [12] K. S. Lee *et al.*, "Spherical indentations on hafnium carbide-and silicon-carbide-coated carbon-carbon composites after thermal shock test in air," *Ceramics International*, vol. 46, no. 13, pp. 21233–21242, 2020.
- [13] P. Ghabezi and N. M. Harrison, "Indentation characterization of glass/epoxy and carbon/epoxy composite samples aged in artificial salt water at elevated temperature," *Polymer Testing*, p. 107588, 2022.
- [14] N.-V. Nguyen, T.-H. Pham, and S.-E. Kim, "Strain rate sensitivity behavior of a structural steel during low-cycle fatigue investigated using indentation," *Materials Science and Engineering: A*, vol. 744, pp. 490–499, 2019.
- [15] Y. P. Cao and J. Lu, "A new method to extract the plastic properties of metal materials from an instrumented spherical indentation loading curve," *Acta Materialia*, vol. 52, no. 13, pp. 4023–4032, Aug. 2004, doi: 10.1016/j.actamat.2004.05.018.

- [16] M. Zhao, N. Ogasawara, N. Chiba, and X. Chen, "A new approach to measure the elastic–plastic properties of bulk materials using spherical indentation," *Acta Materialia*, vol. 54, no. 1, pp. 23–32, Jan. 2006, doi: 10.1016/j.actamat.2005.08.020.
- [17] Y. Cao, X. Qian, and N. Huber, "Spherical indentation into elastoplastic materials: Indentation-response based definitions of the representative strain," *Materials Science and Engineering: A*, vol. 454, pp. 1–13, 2007.
- [18] N. Ogasawara, N. Chiba, and X. Chen, "A simple framework of spherical indentation for measuring elastoplastic properties," *Mechanics of materials*, vol. 41, no. 9, pp. 1025–1033, 2009.
- [19] J.-H. Ahn and D. Kwon, "Derivation of plastic stress–strain relationship from ball indentations: Examination of strain definition and pileup effect," *Journal of Materials Research*, vol. 16, no. 11, pp. 3170–3178, 2001.
- [20] E. Jeon, J.-Y. Kim, M.-K. Baik, S.-H. Kim, J.-S. Park, and D. Kwon, "Optimum definition of true strain beneath a spherical indenter for deriving indentation flow curves," *Materials science and Engineering: A*, vol. 419, no. 1–2, pp. 196–201, 2006.
- [21] F.-Y. Huang, Y.-W. Liu, and J.-C. Kuo, "Uncertainties in the representative indentation stress and strain using spherical nanoindentation," *Applied Nanoscience*, vol. 11, no. 3, pp. 895–909, 2021.
- [22] M. Idriss, O. Bartier, G. Mauvoisin, and X. Hernot, "Determining the stress level of monotonic plastically pre-hardened metal sheets using the spherical instrumented indentation technique," *Journal of Mechanical Science and Technology*, vol. 33, no. 1, pp. 183–195, 2019.
- [23] C. Moussa, X. Hernot, O. Bartier, G. Delattre, and G. Mauvoisin, "Evaluation of the tensile properties of a material through spherical indentation: definition of an average representative strain and a confidence domain," *Journal of Materials Science*, vol. 49, no. 2, pp. 592–603, 2014.
- [24] C. Moussa, X. Hernot, O. Bartier, G. Delattre, and G. Mauvoisin, "Identification of the hardening law of materials with spherical indentation using the average representative strain for several penetration depths," *Materials Science and Engineering: A*, vol. 606, pp. 409–416, 2014.
- [25] Y. Kan, Y. Wu, L. Ren, and H. Chen, "A Simple Method for Measuring Plastic Properties of Power Hardening Metals via the Indentation Curve with a Large Depth," *Advances in Materials Science and Engineering*, vol. 2020, 2020.
- [26] T. Zhang, S. Wang, and W. Wang, "A comparative study on uniaxial tensile property calculation models in spherical indentation tests (SITs)," *International Journal of Mechanical Sciences*, vol. 155, pp. 159–169, 2019.
- [27] M. Wang and J. Wu, "Identification of plastic properties of metal materials using spherical indentation experiment and Bayesian model updating approach," *International Journal of Mechanical Sciences*, vol. 151, pp. 733–745, 2019.
- [28] T. Zhang, S. Wang, and W. Wang, "Method to determine the optimal constitutive model from spherical indentation tests," *Results in physics*, vol. 8, pp. 716–727, 2018.
- [29] T.-H. Pham, Q.-M. Phan, and S.-E. Kim, "Identification of the plastic properties of structural steel using spherical indentation," *Materials Science and Engineering: A*, vol. 711, pp. 44–61, 2018.
- [30] N.-V. Nguyen, J. J. Kim, and S.-E. Kim, "Methodology to extract constitutive equation at a strain rate level from indentation curves," *International Journal of Mechanical Sciences*, vol. 152, pp. 363–377, 2019.
- [31] L. Meng, P. Breitenkopf, B. Raghavan, G. Mauvoisin, O. Bartier, and X. Hernot, "Identification of material properties using indentation test and shape manifold learning approach," *Computer Methods in Applied Mechanics and Engineering*, vol. 297, pp. 239–257, 2015.
- [32] L. Meng, B. Raghavan, O. Bartier, X. Hernot, G. Mauvoisin, and P. Breitenkopf, "An objective meta-modeling approach for indentation-based material characterization," *Mechanics of Materials*, vol. 107, pp. 31–44, 2017.

- [33] M. Wang, J. Wu, Y. Hui, Z. Zhang, X. Zhan, and R. Guo, "Identification of elastic-plastic properties of metal materials by using the residual imprint of spherical indentation," *Materials Science and Engineering: A*, vol. 679, pp. 143–154, 2017.
- [34] L. Meng, P. Breitskopf, B. Raghavan, G. Mauvoisin, O. Bartier, and X. Hernot, "On the study of mystical materials identified by indentation on power law and Voce hardening solids," *International Journal of Material Forming*, vol. 12, no. 4, pp. 587–602, 2019.
- [35] A. Albayda, O. Bartier, X. Hernot, and G. Mauvoisin, "Identification de la déformation représentative et de la loi d'écrouissage des matériaux avec l'indentation sphérique en se basant sur un modèle de gradient de dureté," *Matériaux & Techniques*, vol. 110, no. 2, p. 205, 2022.
- [36] A. Yonezu, K. Yoneda, H. Hirakata, M. Sakihara, and K. Minoshima, "A simple method to evaluate anisotropic plastic properties based on dimensionless function of single spherical indentation—Application to SiC whisker-reinforced aluminum alloy," *Materials Science and Engineering: A*, vol. 527, no. 29–30, pp. 7646–7657, 2010.
- [37] H. U. I. Yu, J. Wu, M. Wang, X. Zhan, and F. A. N. He, "Equivalent strain hardening exponent of anisotropic materials based on spherical indentation response," *Transactions of Nonferrous Metals Society of China*, vol. 29, no. 1, pp. 77–87, 2019.
- [38] X. Zhan *et al.*, "A new modified ECM approach on the identification of plastic anisotropic properties by spherical indentation," *Materials & Design*, vol. 139, pp. 392–408, 2018.
- [39] J. Wu, M. Wang, Y. Hui, Z. Zhang, and H. Fan, "Identification of anisotropic plasticity properties of materials using spherical indentation imprint mapping," *Materials Science and Engineering: A*, vol. 723, pp. 269–278, 2018.
- [40] D. Tabor, "Indentation hardness: fifty years on a personal view," *Philosophical Magazine A*, vol. 74, no. 5, pp. 1207–1212, 1996.
- [41] O. Bartier, X. Hernot, G. Mauvoisin, and C. Moussa, "Comparaison entre les déformations représentatives de l'indentation Vickers et de l'indentation sphérique," *Matériaux & Techniques*, vol. 101, no. 3, p. 303, 2013.
- [42] S. Ghosh and G. Das, "Effect of pre-strain on the indentation fracture toughness of high strength low alloy steel by means of continuum damage mechanics," *Engineering Fracture Mechanics*, vol. 79, pp. 126–137, 2012.
- [43] H. Yu and S. J. Chen, "A mixed hardening model combined with the transformation-induced plasticity effect," *Journal of Manufacturing Processes*, vol. 28, pp. 390–398, 2017.
- [44] X. Li, Y. Wang, P. Zhang, B. Li, X. Song, and J. Chen, "Effect of pre-strain on hydrogen embrittlement of high strength steels," *Materials Science and Engineering: A*, vol. 616, pp. 116–122, 2014.
- [45] D. Zhao, B. Zhu, S. Wang, Y. Niu, L. Xu, and H. Zhao, "Effects of pre-strain on the nanoindentation behaviors of metallic glass studied by molecular dynamics simulations," *Computational Materials Science*, vol. 186, p. 110073, 2021.
- [46] J.-Y. Kim, S.-K. Kang, J. R. Greer, and D. Kwon, "Evaluating plastic flow properties by characterizing indentation size effect using a sharp indenter," *Acta Materialia*, vol. 56, no. 14, pp. 3338–3343, 2008.
- [47] M. Idriss, O. Bartier, G. Mauvoisin, and X. Hernot, "A phenomenological study of the influence of the hardening type on the indentation Fh cyclic curve," *International Journal of Mechanical Sciences*, vol. 197, p. 106336, 2021.
- [48] P. Brammer, X. Hernot, G. Mauvoisin, O. Bartier, and S.-S. Sablin, "A method to take account of the geometrical imperfections of quasi-spherical indenters," *Materials & Design*, vol. 49, pp. 406–413, 2013.
- [49] P. Brammer, G. Mauvoisin, O. Bartier, X. Hernot, and S.-S. Sablin, "Influence of sample thickness and experimental device configuration on the spherical indentation of AISI 1095 steel," *Journal of Materials Research*, vol. 27, no. 1, pp. 76–84, 2012.

- [50] G. Mauvoisin, "Continuous or instrumented indentation device with convex bearing surface and use thereof, particularly for metal sheet indentation. France Patent (2008) FR2008005619, International Patent WO2010/029179 (A1) // EP 2335044 B1 // US 2011/0174036 A1.," US8621903B2, Jan. 07, 2014 Accessed: Jan. 10, 2021. [Online]. Available: <https://patents.google.com/patent/US8621903B2/zh>
- [51] O. Bartier, X. Hernot, and G. Mauvoisin, "Theoretical and experimental analysis of contact radius for spherical indentation," *Mechanics of Materials*, vol. 42, no. 6, pp. 640–656, Jun. 2010, doi: 10.1016/j.mechmat.2010.03.003.
- [52] M. Yetna N'Jock, F. Roudet, M. Idriss, O. Bartier, and D. Chicot, "Work-of-indentation coupled to contact stiffness for calculating elastic modulus by instrumented indentation," *Mechanics of Materials*, vol. 94, pp. 170–179, Mar. 2016, doi: 10.1016/j.mechmat.2015.12.003.
- [53] M. Idriss, "Apport de l'indentation instrumentée dans la caractérisation mécanique des tôles métalliques destinées à l'emboutissage: influence de l'écroissage," PhD Thesis, Rennes 1, 2015.
- [54] E. ISO, "6892-1. Metallic materials-Tensile testing-Part 1: Method of test at room temperature," *International Organization for Standardization*, 2009.
- [55] S. Thuillier and P.-Y. Manach, "Comparison of the work-hardening of metallic sheets using tensile and shear strain paths," *International Journal of Plasticity*, vol. 25, no. 5, pp. 733–751, 2009.
- [56] X. Chu, L. Leotoing, D. Guines, and E. Ragneau, "Temperature and strain rate influence on AA5086 Forming Limit Curves: experimental results and discussion on the validity of the M-K model," *International Journal of Mechanical Sciences*, vol. 78, pp. 27–34, 2014, doi: 10.1016/j.ijmecsci.2013.11.002.
- [57] E. Silvestre, J. Mendiguren, L. Galdos, and E. S. De Argandoña, "Comparison of the hardening behaviour of different steel families: From mild and stainless steel to advanced high strength steels," *International journal of mechanical sciences*, vol. 101, pp. 10–20, 2015.
- [58] L. Zhonghua and G. Haicheng, "Bauschinger effect and residual phase stresses in two ductile-phase steels: Part I. The influence of phase stresses on the Bauschinger effect," *Metallurgical Transactions A*, vol. 21, no. 2, pp. 717–724, 1990.
- [59] H. Ma and Z. Wang, "The Influence of the Bauschinger Effect on Springback Prediction for Dual Phase Steel," *SAE Transactions*, pp. 181–187, 2006.
- [60] M. Weiss, A. Kupke, P. Y. Manach, L. Galdos, and P. D. Hodgson, "On the Bauschinger effect in dual phase steel at high levels of strain," *Materials Science and Engineering: A*, vol. 643, pp. 127–136, 2015.
- [61] N. Christodoulou, O. T. Woo, and S. R. MacEwen, "Effect of stress reversals on the work hardening behaviour of polycrystalline copper," *Acta Metallurgica*, vol. 34, no. 8, pp. 1553–1562, 1986.
- [62] A. Thakur, S. Nemat-Nasser, and K. S. Vecchio, "Dynamic bauschinger effect," *Acta materialia*, vol. 44, no. 7, pp. 2797–2807, 1996.
- [63] T. Hasegawa, T. Yakou, and S. Karashima, "Deformation behaviour and dislocation structures upon stress reversal in polycrystalline aluminium," *Materials Science and Engineering*, vol. 20, pp. 267–276, 1975.
- [64] F. Yoshida, T. Uemori, and K. Fujiwara, "Elastic–plastic behavior of steel sheets under in-plane cyclic tension–compression at large strain," *International journal of plasticity*, vol. 18, no. 5–6, pp. 633–659, 2002.

